MISCELLANEA GEOGRAPHICA – REGIONAL STUDIES ON DEVELOPMENT
Vol. 27 • No. 4 • 2023 • pp. 202-211 • ISSN: 2084-6118 • DOI: 10.2478/mgrsd-2023-0018

Preliminary geological work, based on remote sensing analysis, using artificially enhanced satellite data

Abstract
This study aims to identify areas that present similar spectral characteristics to collected rock samples through the use of satellite imagery and spectral analysis. The results indicate that pixels marked in the satellite images exhibit similarities to the spectral characteristics of the samples. Misclassified objects or areas may be included in the results due to mixed pixels and spatial resolution limitations. The similarities identified could result from the region's mineral composition of building materials, bare land, or dry vegetation. The averaged spectral curve patterns of the samples show similarity overall, but they are not identical, as reflected by the tenth quantile of the similarity coefficient. This research provides a valuable support tool for preliminary geological assessment, and information relating to vast and challenging-to-access parts of prospective areas for further investigation.

Keywords
Satellite imagery • geology • spectral analysis

Katarzyna Adamek[1], Michał Lupa[1], Andrzej Leśniak[1], Jakub Ryznar[2], Adrian Ochtyra[3], Adriana Marcinkowska-Ochtyra[3], Michał Wyczałek-Jagiełło[4]

[1]Department of Geoinformatics and Applied Computer Science Faculty of Geology, Geophysics and Environmental Protection, AGH University of Krakow, Krakow, Poland
e-mail: kadamek@agh.edu.pl
e-mail: mlupa@agh.edu.pl
e-mail: lesniak@agh.edu.pl

[2]Department of Environmental Analysis, Mapping and Economic Geology, Faculty of Geology, Geophysics and Environmental Protection, AGH University of Krakow, Krakow, Poland
e-mail: ryznar@agh.edu.pl

[3]Department of Geoinformatics, Cartography and Remote Sensing Warsaw, Faculty of Geography and Regional Studies, University of Warsaw, Warsaw, Poland
e-mail: adrian.ochtyra@uw.edu.pl
e-mail: adriana.marcinkowska@uw.edu.pl

[4]Geomatic Michał Wyczałek-Jagiełło, Poznan, Poland
e-mail: michal@wyczalek.pl

Received: 26 July 2023
Accepted: 2 October 2023

Introduction

Many studies have shown the usefulness of remote sensing (RS) methods in various aspects of geological exploration and related research. These methods constitute an essential foundation for the initial recognition of many geological problems; they offer many characteristics and possibilities, and have the advantage of high data availability. Several studies have introduced effective remote sensing methods in geology (Sabins Jr 1986; Gupta 2017).

Examples of research on the use of satellite imagery can be found in many publications, indicating the usefulness of RS in geological applications. A review of geological mapping with multi- and hyperspectral data was presented by Van de Meer (2012). Ruisi, Min & Jianping (2011) described remote sensing methods, such as the interpretation of satellite imagery, that can serve the purpose of understanding regional tectonics and be used more broadly for preliminary geological interpretation. Rockwell (2012 and 2013) presented excellent work on using Landsat 7 and Advanced Spaceborne Thermal Emission and Reflection Radiometer (ASTER) imagery for the automatic regional analysis of surface mineralogy. The outputs derived from the automated procedure exhibit favourable characteristics for effectively utilizing mineral resources. Satellite remote sensing methods in mineral prospecting were proven effective by Lupa et al. (2020), where the authors used Landsat 8 data to narrow down the possible areas of mineral occurrence. They combined Landsat 8 imagery with fieldwork, where samples were collected for remote sensing analyses. Yousefi et al. (2018) described a multidisciplinary approach, combining field samples with spectral analysis and satellite data mapping to recognize hydrothermally altered rocks.

As technology progresses, more and more advanced methods are entering this area of research, providing access to newer and newer data with higher temporal, spectral, and spatial resolution; technologies such as machine learning (ML) are also being used in many areas. A broad review of the application of such methods that support remote sensing for geology problems was presented by Lary et al. (2016), who showed that identifying dust sources and combining ML with remote sensing analysis to map various geological aspects is justified.

Improving the resolution of spectral images is a subject of extensive research, regardless of their intended applications. An example of the general utilization of ML for enhancing imagery can be found in work by Collins et al. (2017). The authors demonstrated that the application of Learning Convolutional Neural Networks to satellite data from ResourceSat-1 and -2 enables the generation of enhanced data in areas where high-resolution images are

Vol. 27 • No. 4 • 2023 • pp. 202-211 • ISSN: 2084-6118 • DOI: 10.2478/mgrsd-2023-0018

unavailable. Another example can be found in the work of Zhong et al. (2016), which deals with the enhancement of QuickBird satellite imagery resolution using Convolutional Neural Network-based Super-Resolution (SRCNN) and Gram-Schmidt, transforming it through the use of a panchromatic image. A study by Zhang et al. (2019) focused on increasing the resolution of specific channels of Sentinel-2 data from 20 to 10 metres using the SupReME algorithm. The enhanced data is utilized for retrieving the chlorophyll content of summer corn.

Analysing the obtained results allows us to recognize the usefulness of these types of methods. In our study, we introduce and describe a comprehensive method, from the collection of field samples to the generation of maps of prospective areas. The following sections contain sequential descriptions of the research area, a description of the research methodology, including field sampling with samples characteristics, spectral measurements, a description of enhanced Sentinel-2 data, and a complete description of the algorithm to determine the areas containing rock outcrops with minerals of interest that are similar to our collected samples. Next, the results are shown and discussed in relation to geology. The last two sections comprise a discussion of the research carried out and a summary. The study objective is to present an attempt to identify minerals investigated in the field and tested in the laboratory from artificially enhanced resolution satellite images. The research aims to assess the feasibility of using enhanced satellite imagery to identify regions with spectral characteristics similar to specific rock samples. By focusing on the potential challenges posed by increased resolution, and analysing the spectral curve patterns of samples, the study seeks to validate this method as a valuable tool for preliminary geological assessments, especially in remote or inaccessible areas. This type of research is important for initial geological surveys and for areas that will be subjected to more detailed geological surveys.

Study area

The study area is located in the north-eastern part of Rwanda. Figure 1 shows the research area and sample locations presented in this paper.

The Bugarura–Kuluti (BK) area is located in north-eastern Rwanda, around 100 km to the NE of Kigali. The geology of BK comprises Mesoproterozoic phyllites, metapelites, and quartzites of the Pindura and Gikoro groups (Baudet et al. 1989) (Figure 2). At a regional scale, BK is situated on the flanks of the Karehe anticline (Hanon & Rusanganwa 1991). The core of the NW–SE trending anticline has been intruded by Muhazi granite. The Karehe anticline has numerous second-order folds following the same NW–SE trend. Two main discontinuous structures have been mapped in the region: first, NW–SE bedding-parallel fault planes, related to a compressional regime with a shortening direction, oriented NE–SW (Hulsbosch et al. 2017); second, E–W and NE–SW-oriented faults, caused by regional post-compressional stress regimes.

Materials and Methods

The following section presents a description of the samples, their measurements, satellite imagery description, and conducted remote sensing analyses.

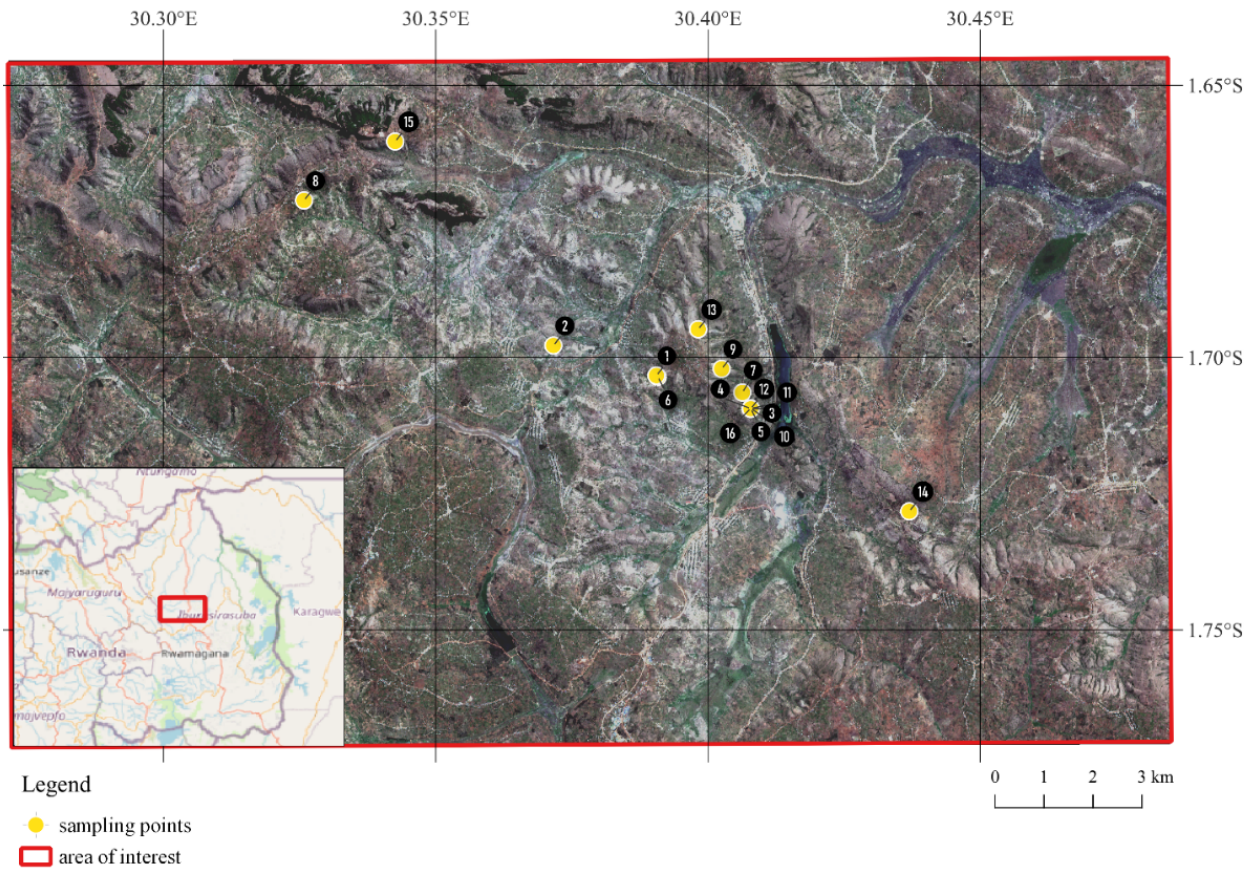

Figure 1. Study area
Source: own elaboration

Vol. 27 • No. 4 • 2023 • pp. 202-211 • ISSN: 2084-6118 • DOI: 10.2478/mgrsd-2023-0018

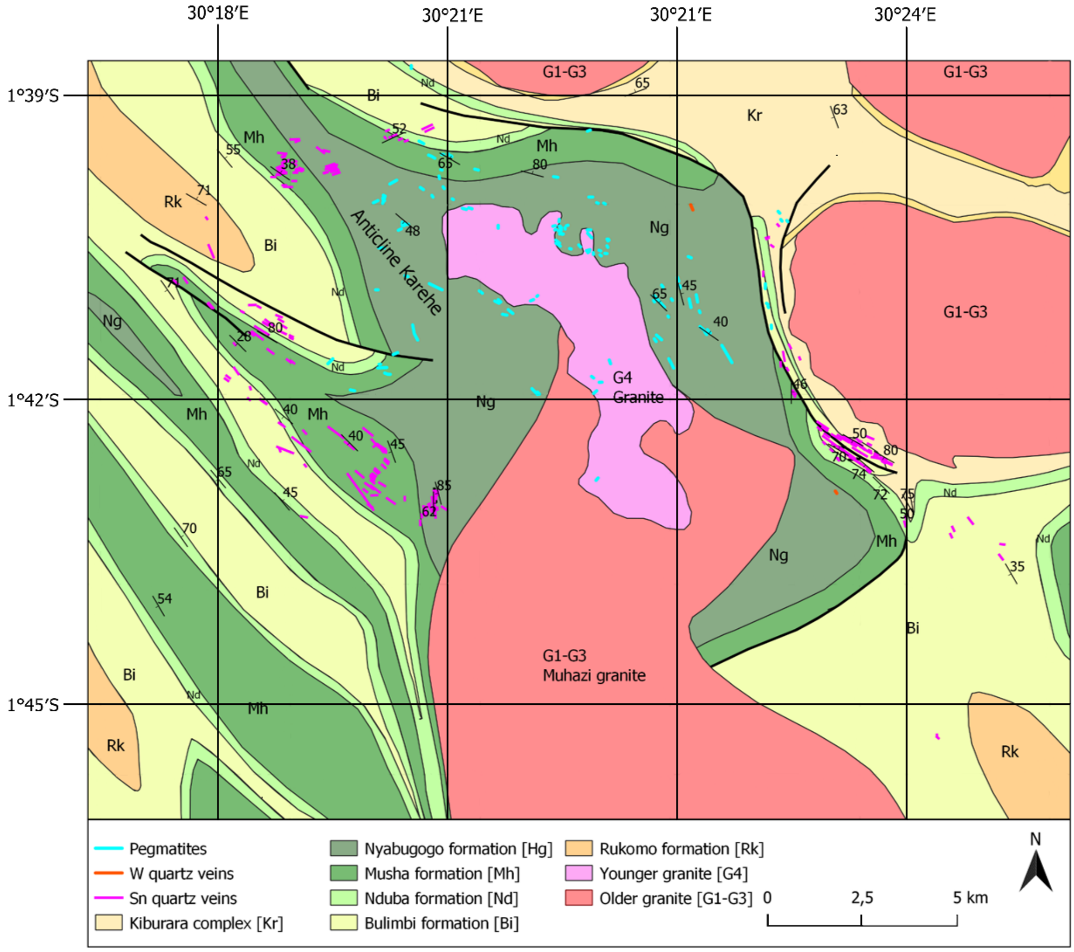

Figure 2. Geological setting of Bugarura and Kuluti with cassiterite Sn mineralization age (numbers on the map). Modified after Hanon & Rusanganwa (1991)

Materials

Samples collection, preparation, and measurements

Sixteen samples from the research area were collected to analyse using remote sensing methods (Table 1).

The first step in the analysis was to perform measurements with the Malvern Panalytical ASD FieldSpec 4 Standard Resolution (SR) hyperspectral spectroradiometer. The spectroradiometer parameters are: Spectral resolution: 3 nm @ 700 nm, 10 nm @ 1400/2100 nm; EM Wavelengths: 350 nm–2500 nm.

Measurements were made using a contact probe with its source of radiation. They were performed while considering the characteristics of the minerals that made up a given rock sample by performing several measurements for each sample. The choice of measurement points on a particular sample were considered based on the minerals visible to the naked eye.

Since the measurements were made in laboratory conditions (and not in situ), the determination of spectral characteristics had to be carried out for dry and wet samples, thus imitating the possible conditions that may have occurred during the satellite's pass.

Examples of the results from the measurements carried out are shown in Figure 3, for the dry sample (Figure 3A) and the wet sample (Figure 3B), successively. Measurements were made for the same area of the sample.

Satellite image and its enhancement

Images from Sentinel-2 were chosen; this is a suitable satellite for this analysis due to its spectral and spatial resolution, as well as the availability of its images of the research area. Sentinel-2 is a satellite of the European Space Agency ESA, operating since 2015 (Sentinel-2A), and is currently on a tandem mission (Sentinel-2B).

One of the basic (and crucial) criteria for selecting imagery analysis is the cloud coverage parameter that should be, in this case, as low as possible. In addition, it is important to minimize the impact of the season of the year or the growing season on the reliability of the measurement, in order to minimize the impact of the atmosphere and vegetation. For this reason, the decision regarding the choice of display should always be preceded by an analysis of the climate in the research area. Different dates will be appropriate for the analysis performed for different regions of the world. Based on this, the selected image was acquired by the Sentinel-2 satellite in August 2018 with the tile number T35MRU.

The accuracy of the analysis depends on two resolutions – spectral and spatial. The 10x10-metre pixel size may cause the formation of mixed pixels because the research area is covered by vegetation, which may lead to a decrease in the quality of the analysis. Therefore, the available artificial intelligence methods were used to enhance the resolution of images in order to increase the accuracy of the analysis by reducing the pixel size from 10

Vol. 27 • No. 4 • 2023 • pp. 202-211 • ISSN: 2084-6118 • DOI: 10.2478/mgrsd-2023-0018

Table 1. List of samples. Source: own elaboration

ID	Host rock	Mineral composition	Number of measurements (dry sample)
1	Altered granite	Quartz, feldspars, kaolinite, muscovite	2
2	Weathered granite	Feldspars, muscovite, biotite	5
3	Muscovite schist with tourmaline	Muscovite, tourmaline, clay minerals	6
4	Pegmatite	Kaolinite, quartz, muscovite	3
5	Pegmatite	Quartz, kaolinite, muscovite	2
6	Muscovite	Muscovite	2
7	Pegmatite	Mainly kaolinite + muscovite	2
8	Pegmatite	Kaolinite, quartz + very fine muscovite	3
9	Pegmatite	Kaolinite, quartz, muscovite	4
10	Greisen	Quartz, muscovite	2
11	Pegmatite	Kaolinite, quartz, muscovite	3
12	Tourmaline	Tourmaline + muscovite	4
13	Pegmatite	Kaolinite, muscovite, quartz	3
14	Tourmaline	Tourmaline	2
15	Quartz with tourmaline	Quartz, tourmaline	3
16	Pegmatite	Kaolinite, quartz, muscovite	4

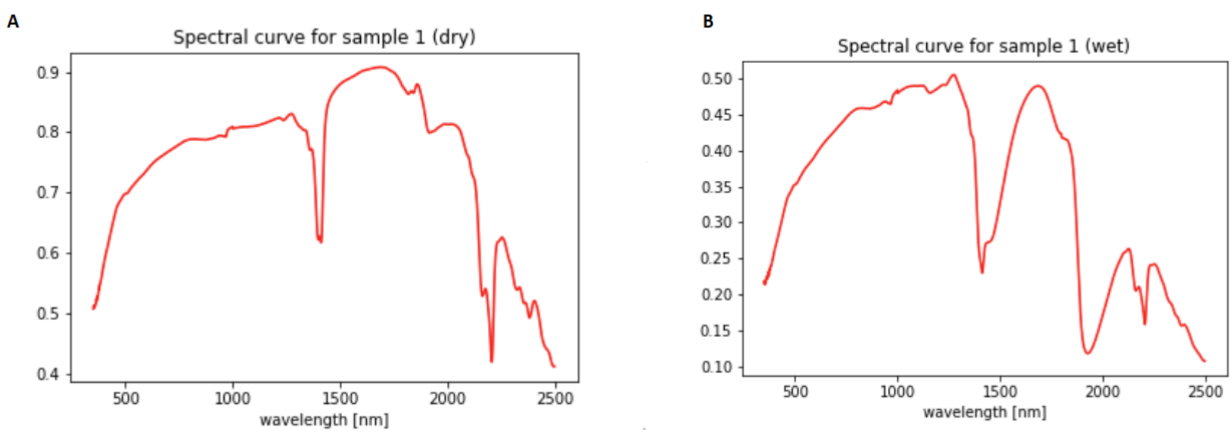

Figure 3. (A) Spectral curve measured from spectroradiometer for sample 1 in the dry case and (B) in the wet case Source: own elaboration

to 2.5 metres. This procedure may increase the reliability of the analysis and reduce the number of mixed pixels. The image with the super-resolution (enhanced beyond its original resolution) resulted from an algorithm provided by the GEOMATIC company. Enhancement was provided for eight bands (B2, B3, B4, B5, B6, B7, B8, and B8a). B1, B9, and B10, called atmospheric bands, were removed from the datasets, and the eight remaining bands were finally used for analysis.

The resolution enhancement was implemented initially by matching the spatial resolution of 20-metre bands to the base 10-metre bands using multi-criteria pansharpening. The matching of the spatial resolution is achieved by employing artificial intelligence and incorporating information obtained from the 10-metre bands. Subsequently, the image undergoes object reconstruction utilizing the RRDN (Residual-in-Residual Dense Network) technique and a model devised by GEOMATIC, constructed upon a dataset of 400,000 pairs of images. RRDN is a deep learning model often used for Single Image Super-Resolution (SISR). The architecture of RRDN incorporates Residual-in-Residual (RIR) blocks with dense connections. The RIR blocks are designed to ease the flow of information and gradients through the network, facilitating the training of deep networks. The dense connections within these blocks also ensure that the network can learn a rich set of features from the input data. When applied to multispectral satellite imagery, super-resolution techniques such as RRDN can be extremely beneficial in increasing the spatial resolution of the images across different spectral bands (Zhang 2018). Lastly, the resulting image is subjected to a tonal alignment process to ensure optimal tonal consistency with the original/input images. The geometric

Vol. 27 • No. 4 • 2023 • pp. 202-211 • ISSN: 2084-6118 • DOI: 10.2478/mgrsd-2023-0018

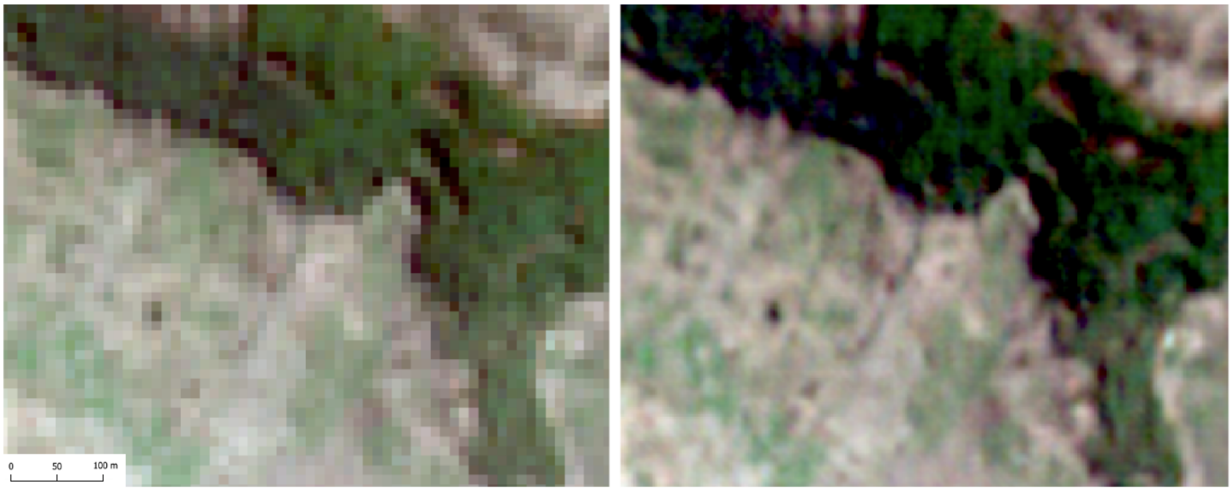

Figure 4. Comparison of image quality for Sentinel-2 original data (left) and enhanced data (right)
Source: own elaboration

and radiometric characteristics of the resultant images are of high value. An example of the quality of the display being improved is shown in Figure 4.

Methods

Correlation of measurements and satellite data

The data, statistically tested by correlation, consisted of spectral measurements with multispectral images were used to determine the average reflectance values in the electromagnetic wave spectrum ranges corresponding to the spectral bands of the satellite (in this case Sentinel-2B). Correlation was performed in two steps.

The first stage was to determine the spectral mean for the measurements performed within a single field sample. The second step was to calculate the spectral average for the reflectance in the ranges corresponding to the spectral bands of the Sentinel-2B images.

As mentioned earlier, measurements were also made in the wet variants of the samples. Therefore, the correlation was performed separately for dry and wet samples.

Similarity coefficient

The similarity coefficient was implemented to find areas on satellite imagery with similar spectral characteristics to those presented by the collected samples. The similarity coefficient sim (k) is calculated for each pixel of the studied area. This makes it possible to compare the averaged reflectance in selected spectral bands to the reflectance of the spectrometer based on the angular distance between two n-dimensional vectors (in our case, n = 8):

$$sim(k) = arc\ \cos\left(\frac{\sum_{i=1}^{8}(hip_i \times ol_i)}{\sqrt{\sum_{i=1}^{8}(hip_i)^2}\ \sqrt{\sum_{i=1}^{8}(ol_i)^2}}\right)$$

Where: i – band number i = 1, …, 8; hip_i – averaged reflectance measured for the rock sample in given band i; ol_i – reflectance for an analyzed pixel in given band i; k – number of samples.

The similarity coefficient sim(k) was calculated for each measured spectrum and the averaged spectra for a given sample. The highest values of the similarity coefficient indicate the greatest similarity of the reflectance of a given sample to the reflectance obtained from the Sentinel-2B image.

Masking

Obtained images were masked in a few steps to exclude areas that could give false positives – such as vegetated areas, built-up areas, or water-covered areas.

Masking was carried out in several steps to exclude as many undesirable areas as possible:

- NDVI (Normalized Difference Vegetation Index) was calculated as $\frac{(Band\,8\ -\ Band\,4)}{(Band\,8\ +\ Band\,4)}$ (Bannari et al. 1995).

NDVI is used for the definition of pixels describing, for example, vegetation, soil, or water. In order to keep the pixels corresponding to the discovered rocks and remove those that probably represent water and vegetation, all of the NDVI indicator values other than 0.05 to 0.35 were marked as pixels to be excluded from the analysis.

- OSM (OpenStreetMap) data was used to mask all classes describing either water or buildings. The selected classes were allotment, building, canal, cemetery, commercial property, drain, farm, farmland, forest, grass, hamlet, health, industrial, meadow, military, nature_reserve, orchard, park, reservoir, residential, river, riverbank, scrub, stream, suburb, town, water, wetland, and village. These were converted from polygons to raster, and marked for exclusion from further analysis.
- Iso Cluster Unsupervised Classification from Esri ArcGIS Desktop was run on RGB composition, and the classes describing water and buildings were masked.

Selecting the highest values of the similarity coefficient

The range of similarity values was divided into 10 classes, according to 10 quantiles, in order to select the most significant values. The pixels in the last of the 10 classes of the similarity coefficient were considered as the places where minerals were most likely to occur. Choosing the highest similarity coefficient makes it possible to map the location of each tested sample.

The analyses were conducted on the rocks in their dry state since the land was dry on the date of the image. The subsequent analysis should therefore include only the dry variant.

Vol. 27 • No. 4 • 2023 • pp. 202-211 • ISSN: 2084-6118 • DOI: 10.2478/mgrsd-2023-0018

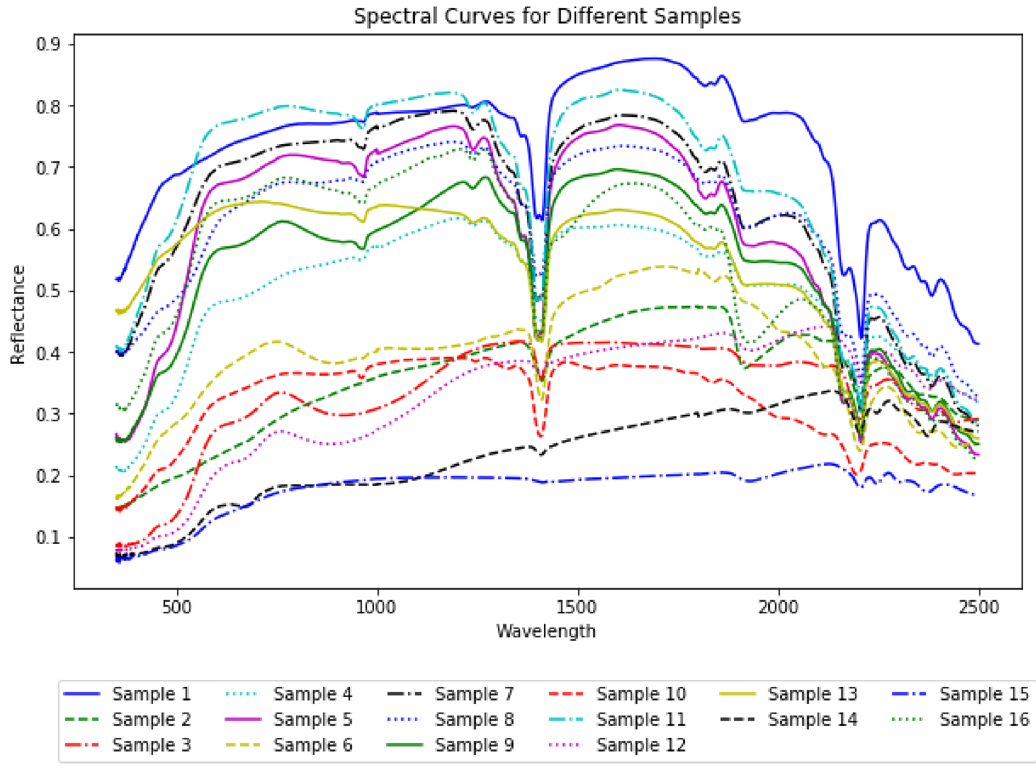

Figure 5. Spectral curves obtained for all samples
Source: own elaboration

Results

Spectral curves, obtained with a spectroradiometer contact probe, are shown in Figure 5. Sample 1 (quartz, feldspars, kaolinite, muscovite) and sample 2 (feldspars, muscovite, biotite) have a similar initial course of the spectral curve (350–1750 nm), but for higher wavelengths, it differs due to a slightly different mineral composition of the sample. Sample 3 (muscovite, tourmaline, clay minerals) and sample 6 (muscovite) show a similar course of spectral curves, probably due to the presence of muscovite in both tested samples. Sample 4 (kaolinite, quartz, muscovite), sample 5 (quartz, kaolinite, muscovite), sample 7 (mainly kaolinite + muscovite), sample 8 (kaolinite, quartz + very fine muscovite), sample 9 (kaolinite, quartz, muscovite), sample 10 (quartz, muscovite), sample 11 (kaolinite, quartz, muscovite), sample 13 (kaolinite, muscovite, quartz), and sample 16 (kaolinite, quartz, muscovite) have similar spectral curves. This is most likely the result of a similar mineral composition, which consists of different proportions of kaolinite, quartz, and muscovite. The last group of similar spectral curves consists of sample 12 (tourmaline + muscovite), sample 14 (tourmaline), and sample 15 (quartz, tourmaline), where the dominant minerals are tourmalines.

The curves presented in Figure 6 show averaged spectral curves for the Sentinel-2B satellite bands.

The curves for sample 1 (quartz, feldspars, kaolinite, muscovite) and sample 2 (feldspars, muscovite, biotite) differ in value but maintain a similar general trend. Both samples contain feldspar and muscovite, and they differ in that sample 1 contains quartz and kaolinite, while sample 2 contains biotite, which may be a sufficient reason for the difference in values. As observed in Figure 7, the indicated regions for sample 1 and sample 2 are similar; however, they differ slightly in terms of surface area and the locations of the tenth quantile pixels. This discrepancy arises from the similar progression of the initial spectral curves, which ultimately diverge in the second part of the curves.

Sample 4 (kaolinite, quartz, muscovite) and sample 9 (kaolinite, quartz, muscovite) are examples of two similar measurements. They exhibit a similar pattern in the curves (Figure 6). The similarity coefficient yields very close results for the tenth quantile, as depicted in Figure 8. The areas highlighted by the indicator for sample 4 and sample 9 are highly similar, indicating the successful functioning of the mechanism for identifying similar areas.

Samples 14 (tourmaline) and 15 (quartz, tourmaline) exhibit almost identical spectral curve patterns after averaging. The results for the similarity coefficient are shown in Figure 9. It can be observed that the indicated regions are highly similar – nearly the same.

Discussion

The application of remote sensing in geological mapping has been substantiated by numerous studies, such as Kruse et al. (1993), Van der Meer et al. (2012), and Bedini (2011). In the Kruse et al. (1993) study, the Spectral Image Processing System (SIPS) showed the importance of real-time visualization and analysis of imaging spectrometer data, even though advancements since its introduction may have superseded its capabilities. Bedini (2011) implemented the practical application of HyMap and ASTER satellite data for mineral mapping in Greenland, illustrating the power of combined satellite data in geological mapping, although its success may be region-specific. In essence, these studies highlight the significant potential of remote sensing in geological mapping.

Vol. 27 • No. 4 • 2023 • pp. 202-211 • ISSN: 2084-6118 • DOI: 10.2478/mgrsd-2023-0018

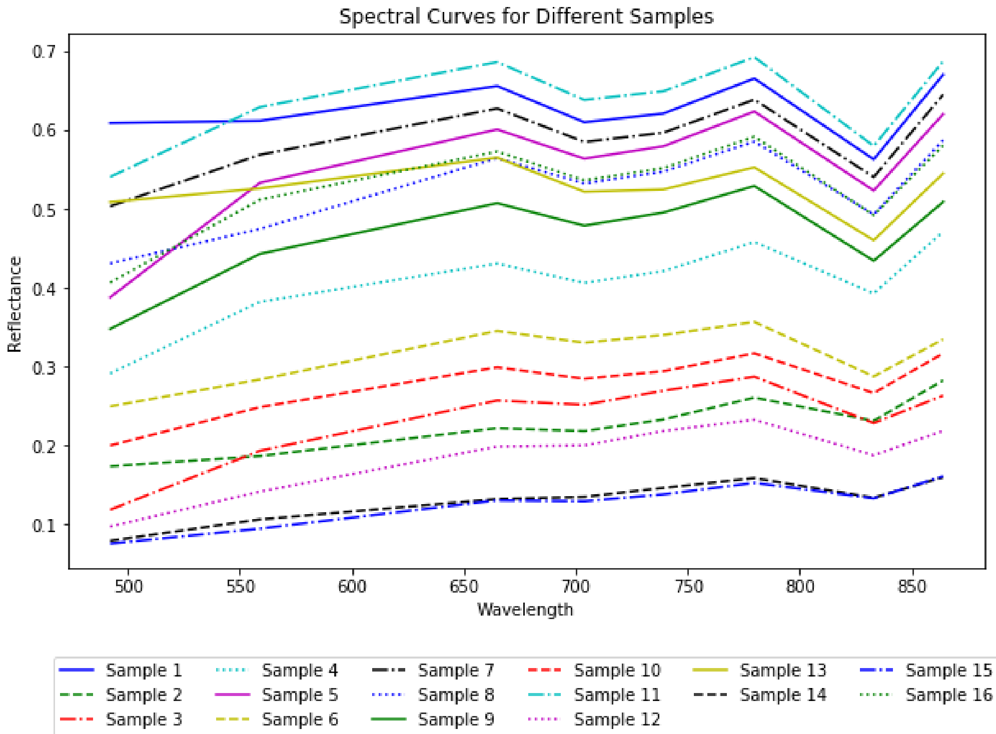

Figure 6. Spectral curves obtained for all samples, averaged for Sentinel-2B bands
Source: own elaboration

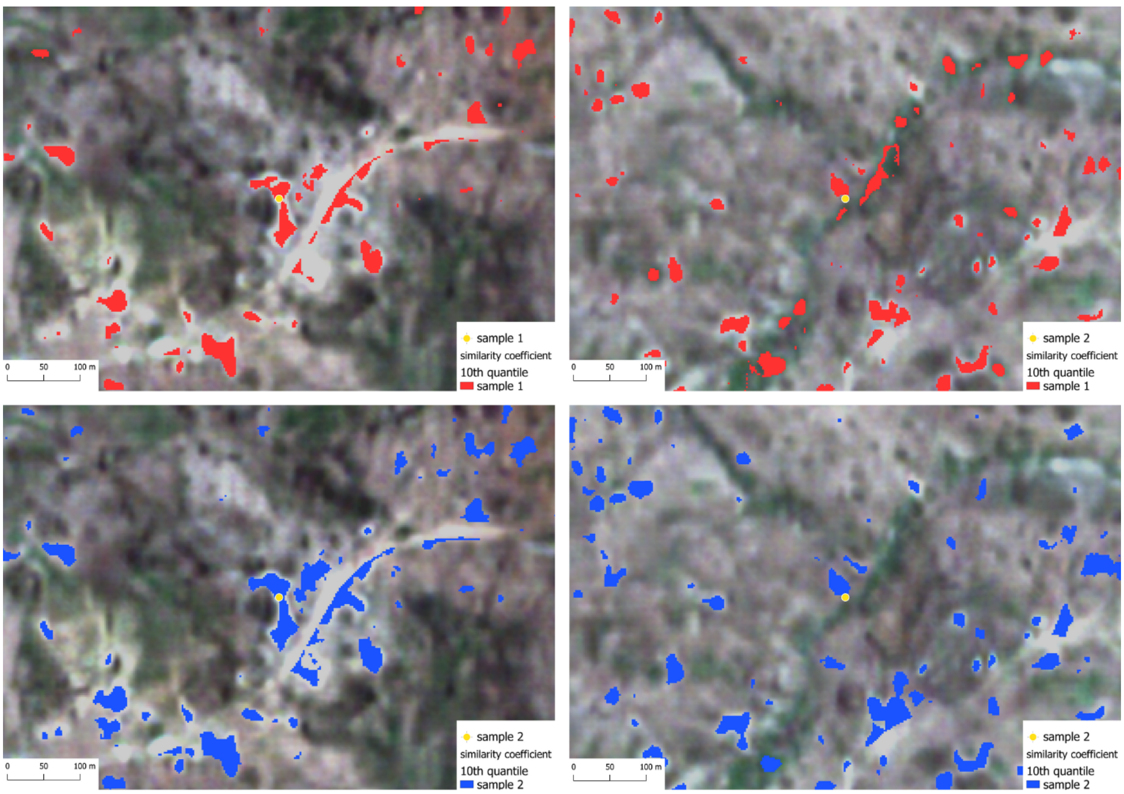

Figure 7. Similarity coefficient for samples 1 and 2
Source: own elaboration

Vol. 27 • No. 4 • 2023 • pp. 202-211 • ISSN: 2084-6118 • DOI: 10.2478/mgrsd-2023-0018

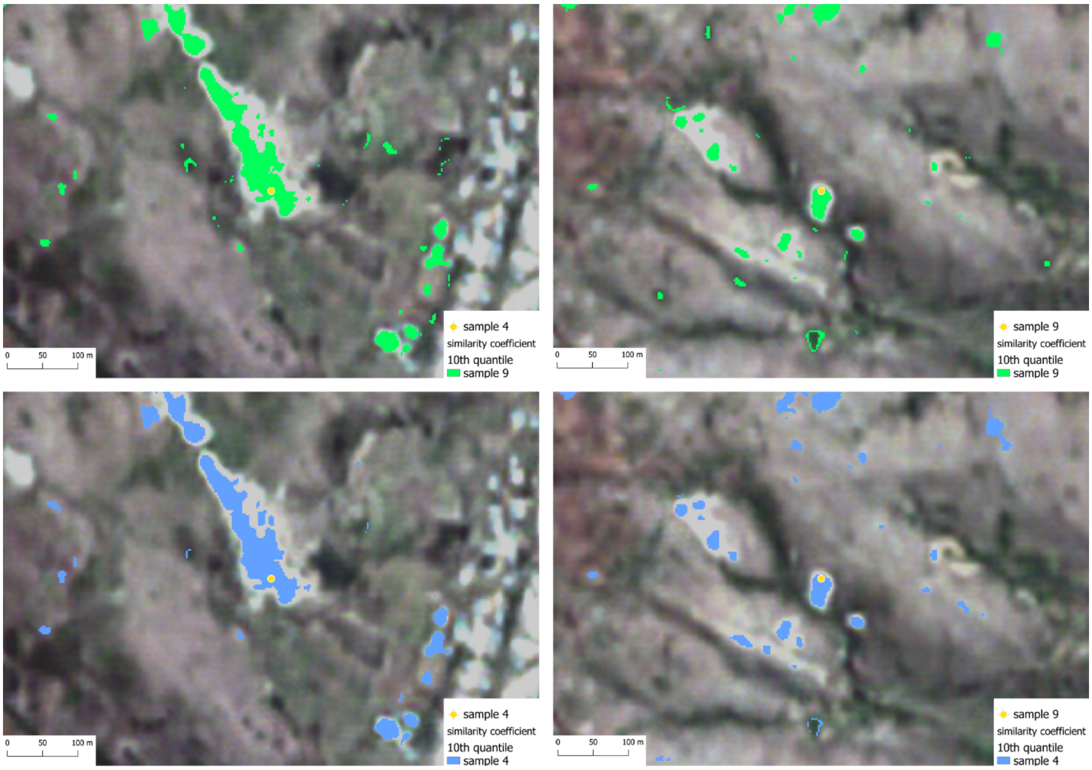

Figure 8. Similarity coefficient for samples 4 and 9
Source: own elaboration

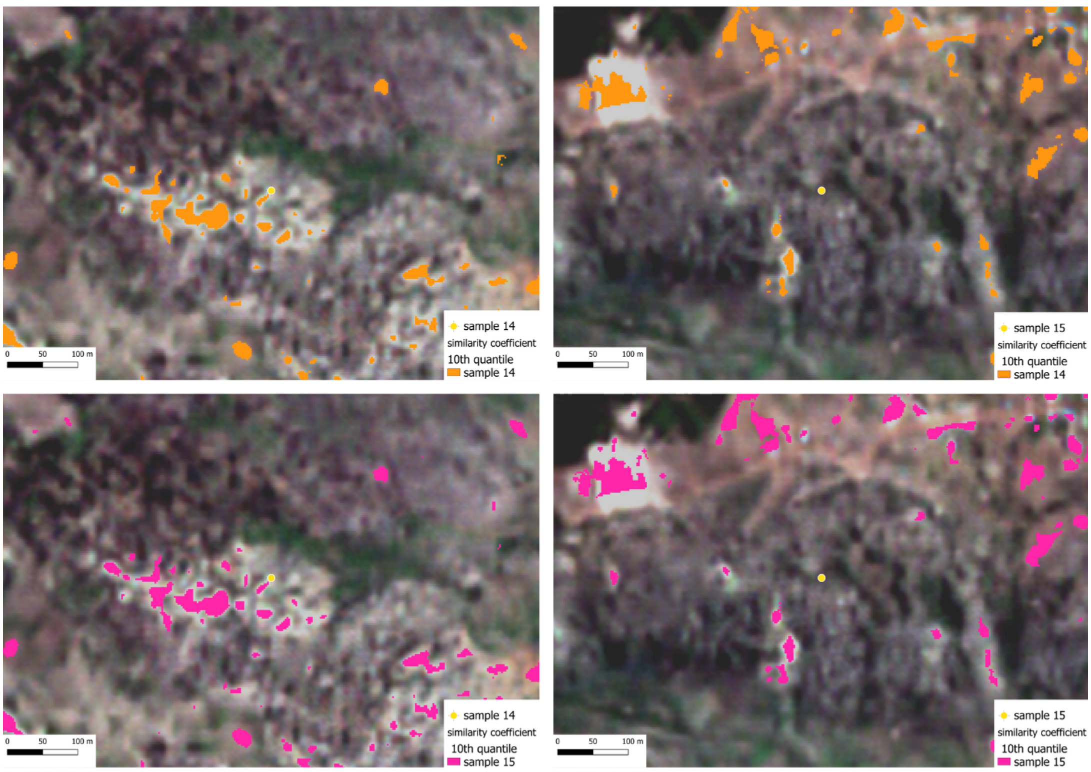

Figure 9. Similarity coefficient for samples 14 and 15
Source: own elaboration

Vol. 27 • No. 4 • 2023 • pp. 202-211 • ISSN: 2084-6118 • DOI: 10.2478/mgrsd-2023-0018

A more specific application of remote sensing, which has also been employed in this publication, involves the utilization of spectral curves, measured in the laboratory, from collected rock samples and satellite data. Several papers emphasize the importance of satellite data and spectral curves in identifying and mapping geological features and minerals in diverse regions. Mars & Rowan (2011) examine the application of ASTER data in the study of the Khanneshin carbonatite volcano in Afghanistan. The researchers successfully identify minerals and create lithologic maps by comparing satellite imagery with ground-based spectral curves. This study underscores the efficacy of combining ASTER data with spectral analysis techniques in order to characterize geological features. In another study, Parashar et al. (2016) utilized Hyperion data to map minerals in the Aravalli fold belt, located in south-eastern Rajasthan. Rock samples from the region were analysed under laboratory conditions using a Spectroradiometer, and the resulting spectra were cross-verified with the USGS spectral library. The imagery underwent standard processing, including atmospheric correction, noise reduction, and visualization techniques, and the Spectral Angle Mapper technique was employed to identify minerals from the carbonate, clay, and silicate groups.

These articles collectively underscore the significance of spectral analysis in geological investigations. They demonstrate the effectiveness of using satellite data, along with spectral curves, in mineral identification, geological mapping, and environmental monitoring. These studies demonstrate the validity of the research presented in this article. The novel aspect of the above is the utilization of Sentinel-2 data with enhanced resolution, which enables even more precise results to be attained.

Few studies compare field-collected rock samples with satellite imagery to identify areas of potential occurrence of specific rock types. Mars and Rowan (2011) compared a sand sample with ASTER data. The spectral curve was measured using an Analytical Spectral Device (ASD), which records electromagnetic waves in the range of 400–2500 nm, representing a slight difference compared to the ASD FieldSpec 4 spectrometer we employed, which has a range of 350–2500 nm. The obtained spectral curve was resampled to match the spectral channels of ASTER. However, in the conducted comparison, a geological map of the area was utilized, which was not the case in our study. The assumption of the research presented in this work is the absence of the need to rely on additional data such as geological maps.

Another similar example of utilizing rock samples was presented by Crowley, Hubbard & Mars (2003). They focused on the potential use of airborne and satellite data to determine the sources of debris flow, employing NASA's Airborne Visible/Infrared Imaging Spectrometer (AVIRIS), Hyperion, and ASTER data. The spectral curves of the rock samples were not utilized, as in our study, to search for similar areas. Instead, they were compared with spectra obtained from AVIRIS for sample locations. This aspect of their work is undoubtedly intriguing and will be considered in future research on the algorithm. However, it is worth noting that our study utilizes publicly available data for the entire world, specifically Sentinel-2 data.

The pixels marked in Figures 7, 8, and 9 should be interpreted as spots with spectral characteristics registered on satellite imagery that are most similar to the spectral characteristics of the collected sample.

In the context of the presented results, samples 1 and 2 have successfully pinpointed potential sites of granite occurrence. Samples 9 and 4 were employed to demonstrate the similarity coefficient pertinent to granite. Meanwhile, samples 14 and 15 represent the most probable locations for the occurrence of tourmaline/quartz and tourmaline, respectively. Cross-validation in each of these instances corroborates the accuracy of the results, with samples of analogous material producing highly consistent responses. For instance, the pegmatite collection site for sample 9 was also indicated by the similarity coefficient for sample 4, which was likewise extracted from pegmatite. The sole exception is presented by sample 15, for which the collection site was not indicated by the similarity coefficient due to the site being situated within a region densely covered with vegetation. It can be postulated that, in the absence of such flora, the similarity coefficient would likely have identified a response in that region.

However, it is essential to consider that due to mixed pixels, pixels classified in the quantile class 10 may also include objects and areas adjacent to rock outcrops. Enhanced resolution improves the obtained results but still leaves room for further improvement. Moreover, the pixels showing the similarity of the rock sample to the area in the satellite image may have similar characteristics because the mineral composition of the building materials for houses, roads, or quays could be similar to the mineral composition of the samples. Land and dry vegetation may also show spectral similarity, which is abundant for a selected region of Africa.

After averaging, all the samples exhibit relatively similar spectral curve patterns, indicating similar (though not identical) regions by the tenth quantile of the similarity coefficient. Samples with a more diverse mineral composition would likely yield different responses.

When analysing the obtained results, basic knowledge about the region under study is necessary to avoid making basic errors during interpretation. Research of this type should not be treated as geological mapping per se, but as support during preliminary geological works to provide information on prospective areas for further work and research. From this perspective, conducting such research is extremely important due to the possibility of quickly analysing vast areas, including those difficult to access.

The primary objective of this study was to evaluate the potential of using satellite data, specifically from Sentinel-2B, in conjunction with spectral curves obtained from rock samples, to identify areas with similar geological properties. This objective was substantially achieved, as demonstrated by the alignment of spectral curves between the samples and the corresponding regions in satellite imagery. The discussed case study shows how optical imagery (Copernicus, Sentinel-2) can serve as a basis for developing automatic mineral prospecting maps. Furthermore, it has been demonstrated how the adaptation of deep learning methods allows the resolution of multispectral images to be enhanced, thereby partially mitigating the problems associated with mixed pixels, which are characteristic of areas covered with vegetation. A method of comparing spectral characteristics of in-situ samples with satellite data has also been demonstrated, with the aim of identifying areas where a similar spectral response occurs, consequently indicating a high probability of the presence of rocks with a similar mineral composition.

Conclusion

In conclusion, the marked pixels represent areas on satellite imagery that show spectral characteristics similar to the collected sample. Despite the increased resolution, which undoubtedly positively impacts the obtained results, it is still necessary to consider the possible presence of mixed pixels. Neighbouring objects and areas adjacent to rock outcrops may still be included. The samples exhibit relatively similar spectral curve patterns, indicating comparable regions based on the similarity coefficient. Diverse mineral compositions would likely yield different responses. This research serves as a valuable tool for preliminary geological assessment by identifying prospective areas for further investigation in remote or inaccessible regions.

Vol. 27 • No. 4 • 2023 • pp. 202-211 • ISSN: 2084-6118 • DOI: 10.2478/mgrsd-2023-0018

Acknowledgements

This work was financed within the framework of the statutory research of the AGH-University of Science and Technology, Faculty of Geology, Geophysics, and Environmental Protection.

Data Availability

The data will be available upon submitting a request to the authors.

ORCID

Katarzyna Adamek https://orcid.org/0000-0003-2595-9296
Michał Lupa https://orcid.org/0000-0002-4870-0298
Andrzej Leśniak https://orcid.org/0000-0002-9442-0799
Jakub Ryznar https://orcid.org/0000-0003-0243-3734
Adrian Ochtyra https://orcid.org/0000-0003-4799-8093
Adriana Marcinkowska-Ochtyra https://orcid.org/0000-0002-9080-3899

References

Bannari, A, Morin, D, Bonn, F & Huete, A 1995, 'A review of vegetation indices', *Remote sensing reviews,* vol. 13, no. (1-2), pp. 95–120.

Baudet, D, Hanon, M, Lemonne, E, Theunissen, K, Buyagu, S, Dehandschutter, J, Ngizimana, W, Nsengiyumva, P, Rusanganwa, J & Tahon, A 1989, 'Lithostratigraphie du domaine sédimentaire de la chaîne Kibarienne au Rwanda', *Annales de la Société géologique de Belgique*, vol. 112.

Bedini, E 2011, 'Mineral mapping in the Kap Simpson complex, central East Greenland, using HyMap and ASTER remote sensing data', *Advances in Space Research,* vol. 47, no. 1, pp. 60–73.

Collins, CB, Beck, JM, Bridges, SM, Rushing, JA & Graves, SJ 'Deep learning for multisensor image resolution enhancement', *Proceedings of the 1st Workshop on Artificial Intelligence and Deep Learning for Geographic Knowledge Discovery*, pp. 37–44.

Crowley, J, Hubbard, B & Mars, J 2003, 'Analysis of potential debris flow source areas on Mount Shasta, California, by using airborne and satellite remote sensing data', *Remote Sensing of Environment,* vol. 87, no. 2–3, pp. 345–358.

Gupta, RP 2017, *Remote sensing geology*, Springer, Heidelberg.

Hanon, M & Rusanganwa, J 1991, *Carte Géologique du Rwanda, Feuille Kigali, 1: 100,000 et note explicative*, Département de Géologie et de Minéralogie du Musée royal de l'Afrique Centrale et le Ministère de l'Industrie et de l'Artisanat du Rwanda, Tervuren.

Hulsbosch, N, van Daele, J, Reinders, N, Dewaele, S, Jacques, D & Muchez, P 2017, 'Structural control on the emplacement of contemporaneous Sn-Ta-Nb mineralized LCT pegmatites and Sn bearing quartz veins: Insights from the Musha and Ntunga deposits of the Karagwe-Ankole Belt, Rwanda', *Journal of African Earth Sciences,* vol. 134, pp. 24–32.

Kruse, FA, Lefkoff, A, Boardman, J, Heidebrecht, K, Shapiro, A, Barloon, P & Goetz, A 1993, 'The spectral image processing system (SIPS)—interactive visualization and analysis of imaging spectrometer data', *Remote sensing of environment,* vol. 44, no. 2–3, pp. 145–163.

Lary, DJ, Alavi, AH, Gandomi, AH & Walker, AL 2016, 'Machine learning in geosciences and remote sensing', *Geoscience Frontiers,* vol. 7, no. 1, pp. 3–10.

Lupa, M, Adamek, K, Leśniak, A & Pršek, J 2020, 'Application of satellite remote sensing methods in mineral prospecting in Kosovo, area of Selac', *Gospodarka Surowcami Mineralnymi,* vol. 36, no. 1, pp. 5–22.

Mars, JC & Rowan, LC 2011, 'ASTER spectral analysis and lithologic mapping of the Khanneshin carbonatite volcano, Afghanistan', *Geosphere,* vol. 7, no. 1, pp. 276–289.

van der Meer, FD, van der Werff, HM, van Ruitenbeek, FJ, Hecker, CA, Bakker, WH, Noomen, MF, van Der Meijde,

M, Carranza, EJM, De Smeth, JB & Woldai, T 2012, 'Multi- and hyperspectral geologic remote sensing: A review', *International Journal of Applied Earth Observation and Geoinformation,* vol. 14, no. 1, pp. 112–128.

Parashar, C, Sharma, R, Chattoraj, S, Sengar, V & Champati Ray, P 2016, 'Identification and mapping of minerals by using imaging spectroscopy in southeastern region of Rajasthan', *Conference: SPIE Asia-Pacific Remote Sensing*, New Delhi, India.

Rockwell, BW 2012, 'Description and validation of an automated methodology for mapping mineralogy, vegetation, and hydrothermal alteration type from ASTER satellite imagery with examples from the San Juan Mountains, Colorado', *Scientific Investigations Map*, US Geological Survey, Reston.

Rockwell, BW 2013, 'Automated mapping of mineral groups and green vegetation from Landsat Thematic Mapper imagery with an example from the San Juan Mountains, Colorado', *Scientific Investigations Map*, US Geological Survey, Reston.

Ruisi, Z, Min, Z & Jianping, C 2011, 'Study on Geological Structural Interpretation based on Worldview-2 Remote Sensing Image and Its Implementation', *Procedia Environmental Sciences,* vol. 10, pp. 653–659.

Sabins Jr, F 1986, *Remote sensing: principles and interpretation*, Chevron Oil Field Research Co, United States.

Yousefi, SJ, Ranjbar, H, Alirezaei, S, Dargahi, S & Lentz, DR 2018, 'Comparison of hydrothermal alteration patterns associated with porphyry Cu deposits hosted by granitoids and intermediate-mafic volcanic rocks, Kerman Magmatic Arc, Iran: Application of geological, mineralogical and remote sensing data', *Journal of African Earth Sciences,* vol. 142, pp. 112–123.

Zhang, M, Su, W, Fu, Y, Zhu, D, Xue, J-H, Huang, J, Wang, W, Wu, J & Yao, C 2019, 'Super-resolution enhancement of Sentinel-2 image for retrieving LAI and chlorophyll content of summer corn', *European Journal of Agronomy,* vol. 111, article number 125938.

Zhang, Y, Tian, Y, Kong, Y, Zhong, B & Fu, Y 2018, 'Residual Dense Network for Image Super-Resolution', in *Proceedings of the IEEE Conference on Computer Vision and Pattern Recognition (CVPR)*, pp. 2472–2481.

Zhong, J, Yang, B, Huang, G, Zhong, F & Chen, Z 2016, 'Remote sensing image fusion with convolutional neural network', *Sensing and Imaging,* vol. 17, pp. 1–16.